Laminar and turbulent regime changes in drinking water contact tanks

TAYLOR C. BARNETT[1] AND SUBHAS K. VENAYAGAMOORTHY[2]

[1]Innovyze, Broomfield, Colo.
[2]Department of Civil and Environmental Engineering, Colorado State University, Fort Collins, Colo.

Transitions in flow regimes that can occur in drinking water contact tanks may significantly affect the disinfection efficiency of the system. To demonstrate these effects, the authors investigated the internal velocity fields and flow regime of a drinking water contact tank located in Jamestown, Colo. The baffling factor (BF) of the system fluctuated annually between 0.5 and 0.6 because of a shift in flow regime caused by changes in the flow rate of the system. The authors studied the effects of the regime change from laminar to turbulent flow (or vice versa) using computational fluid dynamics (CFD) models and physical tracer studies. Several inlet modifications were then investigated using CFD to determine which alteration would be most beneficial. Key findings showed that with proper inlet modification, the BF of the system could be stabilized at 0.6 during periods of high or low flow.

Keywords: *baffling factor, contact tank hydraulics, drinking water, laminar flow, turbulent flow*

Internal velocity fields in drinking water disinfection contact tanks can vary greatly depending on, among other parameters, tank geometry, inlet geometry, system flow rate, and water temperature. The velocity field has a direct effect on the hydraulic disinfection efficiency of a treatment system and as such must be taken into account in the design of a highly efficient system (Wang & Falconer, 1998). Until recently contact tanks were designed using empirically derived equations or physical studies (USEPA, 1991). Recent advances in computational fluid dynamics (CFD) have provided deeper insight into the complex hydrodynamics of contact tanks. The use of CFD to investigate the hydrodynamics of contact tanks has previously been validated using several full-scale and laboratory-scale models (Amini et al, 2011; Khan et al, 2006; Templeton et al, 2006; Wang et al, 2003; Brouckaert & Buckley, 1999).

Because chlorination is the most common method of drinking water disinfection used in the United States, numerous inadequately designed systems are at risk of producing cancerous disinfection by-products (Rauen et al, 2012; Wang et al, 2003). Many of these treatment systems are located within small towns or rural areas and provide water to populations of 3,000 or fewer people (and are therefore classified as small systems). Although these small systems provide drinking water to only 18% of the US population, they are responsible for 94% of violations of US Environmental Protection Agency (USEPA) maximum contaminant levels (USEPA, 2011).

In the United States, the USEPA has adopted the method of assigning contact tanks a baffling factor (BF) as a surrogate for hydraulic efficiency. The BF is the ratio of the time at which 10% of the inlet concentration of a tracer is observed at the outlet to the theoretical detention time (TDT) of the system (USEPA, 2003). TDT is determined by assuming plug flow and taking the ratio of the system volume, V, to the average volumetric flow rate, Q. Plug flow as defined by USEPA is when "... water travels through a basin, pipe, or unit process in such a fashion that the entire mass or volume is discharged at exactly the TDT of the unit and no short-circuiting occurs" (USEPA, 2003). This unique wording by USEPA implies that plug flow may occur in both laminar and turbulent flow, despite the significant difference between these flows. Recent studies have shown that few systems achieve a uniform plug flow velocity field; however, those researchers studied only systems in which the flow regime was entirely turbulent (Amini et al, 2011; Zhang et al, 2011a; Zhang et al, 2011b; Baawain et al, 2006).

The hydraulic efficiency of a system can be visualized by a residence time distribution (RTD) curve. An RTD curve can be generated with CFD or physical tracer studies in which the concentration of a passive tracer in the effluent is plotted over time and closely resembles a cumulative distribution function. Systems with a high BF will have a corresponding RTD curve that is similar to a step function, whereas systems that have diffusive flow and low BFs will have RTD curves with very low gradients (i.e., less steepness).

The authors used a serpentine contact tank located in Jamestown, Colo., as the basis for this study. CFD was used to evaluate the hydraulic disinfection efficiency and model the internal velocity fields within the tank; physical tracer studies were used to validate the CFD models. The next section presents a brief discussion of the methodologies used in the CFD simulations and physical tracer studies. The presentation of results is followed by a detailed discussion of how hydraulic disinfection efficiency was affected by several proposed modifications to the tank inlet.

THEORETICAL BASIS

Computational methodology. A finite-volume commercial CFD code[1] was used to solve the Reynolds-averaged Navier–Stokes equations. The renormalization group k-ϵ model was used for the turbulence closure when the Reynolds number of the flow suggested turbulent flow (Pope, 2000). This turbulence model was used because it has been shown to be better than the standard k-ϵ model at handling flows with separation and recirculation zones (ANSYS, 2011; Bradbrook et al, 1998). The pressure field was solved using the standard semi-implicit method for pressure-linked equations, or SIMPLE, algorithm, whereas the first-order upwind method was used for the momentum. Computational models were initialized using a velocity inlet and pressure outlet with the walls treated as a no-slip boundary. The free surface was modeled as a wall with zero shear stress. Each model was allowed to reach a steady-state solution before a transient time scheme was implemented. Once convergence of the steady-state velocity field had been achieved, a transient model was then used to solve for the passive scalar—considered here as any species that can be transported but is nonreactive and has no influence on the flow field—concentration field as it passed through the system. The transport of the passive scalar (e.g., a conservative tracer) was modeled using the advection–diffusion equation given by Eq 1:

$$\frac{DC}{Dt} = \frac{\partial C}{\partial t} + \overline{U} \bullet \nabla C = \nabla \bullet \left(\left(\kappa + \frac{\nu_t}{Sc_t} \right) \nabla C \right) \quad (1)$$

in which DC/Dt is the total time rate of change of concentration, $\partial C/\partial t$ is the local time rate of change of concentration, C is the concentration of the passive scalar, $\overline{U}$ is the transient-state velocity, $\nabla \bullet$ is the divergence operator, ∇ is the gradient operator, κ is the molecular diffusivity of the passive scalar, and ν_t/Sc_t is the turbulent diffusivity of the passive scalar, with ν_t the turbulent eddy viscosity and Sc_t the turbulent Schmidt number. $\overline{U}$ and ν_t were obtained from the transient-state velocity field, whereas the turbulent Schmidt number (Sc_t) was taken as 0.7 (Venayagamoorthy & Stretch, 2010). The concentration of this passive scalar was monitored at the outlet so that RTD curves could then be generated for each system.

A grid independence study was performed to ensure that the flow fields were accurately resolved. Four meshes were constructed that encompassed a range of total volume cells (Table 1). The maximum velocity and BF found with each mesh were used for convergence criteria. The mesh was assumed to have converged on an accurate velocity field when these two parameters approached an asymptote when plotted versus the total number of cells in the mesh. From this study it was found that the mesh containing 166,853 total cells would provide acceptable grid-independent results for the CFD study.

Physical testing methodology. Step-input tracer studies were conducted on the physical system by injecting a solution of lithium chloride into the influent. Lithium chloride was selected as a passive tracer because it is found in drinking water at low background levels. The stock tracer solution of lithium chloride was mixed so that the effluent concentration would not exceed 0.04 mg/L. This tracer solution was injected into the influent via a secondary chlorine injection port located just upstream of the primary chlorine injection port; the effluent samples were collected at the overflow weir. Because the secondary port was not in use for plant operation, the tracer studies were conducted using this port while the plant was operational. The samples collected were analyzed at the Colorado State University Soil, Water, and Plant Testing Laboratory (Fort Collins, Colo.) using inductively coupled plasma/atomic emission spectroscopy.

TABLE 1 Results of the parametric mesh study

Total Number of Volume Cells	Maximum Tank Velocity *ft/min*	BF
304,605	22.51	0.675
166,853	22.91	0.635
67,313	22.86	0.657
79,304	23.18	0.659

BF—baffling factor

METHODOLOGY

The city of Jamestown allowed the use of its drinking water disinfection contact tank for this study. The tank (shown schematically in Figure 1) held approximately 5,000 gal (18,927 L) and was designed to operate at 180,000 gpd (7.9 L/s). However, typical flow rates for the system were between 20,000 gpd (0.88 L/s) in the winter and 80,000 gpd (3.5 L/s) during the summer.

Baseline CFD models. To provide a better understanding of the complex flow hydrodynamics that occurs in the contact tank shown in Figure 1, baseline CFD models were simulated with flow rates of 80,000 gpd (3.5 L/s) and 20,000 gpd (0.88 L/s). The flow depth over the outlet (sharp-crested) weir for these two flow rates were calculated as shown in Eq 2 (Rouse, 1946):

$$Q = \frac{2}{3} \left(0.611 + 0.075 \frac{H_1}{P} \right) \sqrt{2g}\, B H_1^{3/2} \quad (2)$$

in which Q is the system flow rate, H_1 is the flow depth above the weir, P is the weir height, g is the acceleration resulting from gravity, and B is the width of the weir. Eq 2 was used to determine that the flow depth over the weir was 0.25 in. (0.64 cm) for a system flow rate of 20,000 gpd (0.88 L/s) and 0.62 in. (1.58 cm) for a flow rate of 80,000 gpd (3.5 L/s).

Laminar/turbulent study. During normal operation of a chlorine contact tank, the flow is assumed to be primarily turbulent. The CFD models performed for the baseline study were analyzed to determine the flow regime for both the 80,000-gpd (3.5-L/s) and 20,000-gpd (0.88-L/s) cases. In closed-conduit hydraulics, flow is considered laminar if the Reynolds number is approximately less than 2,000 and turbulent when it is well above 4,000. In the current study, the authors adopted the same threshold values for classifying the flow regimes and ensured consistency by using the hydraulic diameter of the tank as the characteristic length scale.

FIGURE 1 Geometry of the Jamestown disinfection contact tank

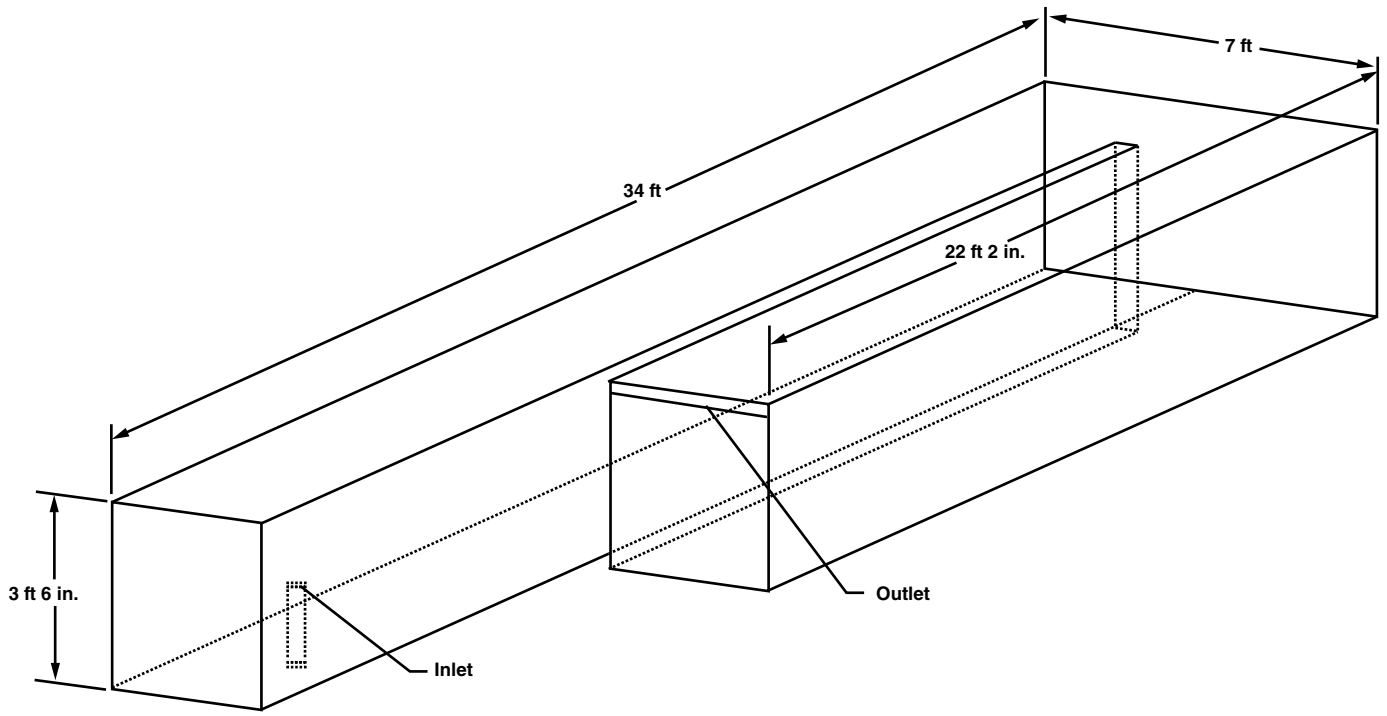

The Reynolds number is a nondimensional ratio of the inertial (momentum) forces to the viscous forces in the flow. Laminar flows have velocity fields that are affected mainly by the molecular viscosity. In a laminar flow, the viscosity of the fluid is the primary source of dissipation of the kinetic energy. Conversely, if a flow is turbulent, the velocity field is affected mainly by the inertial forces, with mixing accomplished by turbulent eddies and large-scale motions, whereas the effects of molecular viscosity are negligible. The enhanced turbulent mixing helps dissipate any high-velocity jets caused by sharp inlets. The Reynolds number is calculated as in Eq 3:

$$Re = \frac{uL}{\nu} \tag{3}$$

in which Re is the Reynolds number, u is the characteristic velocity (fps), L is the characteristic length (ft), and ν is the kinematic (molecular) viscosity of the fluid (sq ft/s).

The Reynolds numbers calculated in this study use a hydraulic diameter of 5.84 ft (1.78 m) for the characteristic length; the kinematic viscosity varied depending on the season. The water temperature fluctuated annually between 40 and 80°F (4.4–26.6°C). This drastic swing in raw water temperature caused the kinematic (molecular) viscosity of water to range from 0.93×10^{-5} sq ft/s (0.86×10^{-6} m^2/s) to 1.66×10^{-5} sq ft/s (1.54×10^{-6} m^2/s) (Munson et al, 2013).

Tank modification study. Three tank modifications were modeled with CFD to determine how the inlet structure could alter the velocity fields. The first option modeled was an idealized case to determine the theoretical maximum increase in BF achievable with only inlet modifications. Figure 2, part A, shows the model geometry for the idealized case. In this configuration the entire front wall of the tank was set as an inlet so that the influent would enter the system uniformly. The results from this model were used to create and model two inlet modifications. The first proposed modification (Figure 2, part B) used a 90-degree elbow on top of the existing inlet to redirect the flow toward the front wall. In the second modification (Figure 2, part C), a tee was placed on top of the inlet to split the flow in two, with 90-degree elbows placed on either end of the tee to direct the flow toward the front wall (as in the previous modification). Both modifications involved pointing the influent toward the front wall to use this wall to dissipate energy from the flow. With the inlets facing the front wall, it was expected that the flow would spread out and mimic the idealized case after hitting the wall.

RESULTS

Baseline models. Tracer studies were conducted on the existing system using flow rates of 20,000 gpd (0.88 L/s) and 80,000 gpd (3.5 L/s) to validate the results from the baseline CFD models. Figure 3, parts A and B, shows the RTD curves generated using the CFD results and data from the lithium chloride tracer studies for the two flow rates. As the tracer studies were being conducted, an anomaly was noticed within the system that had not been accounted for within the CFD simulations. During normal operation, the treated effluent from the contact tank spilled over the

FIGURE 2 Inlet geometries tested

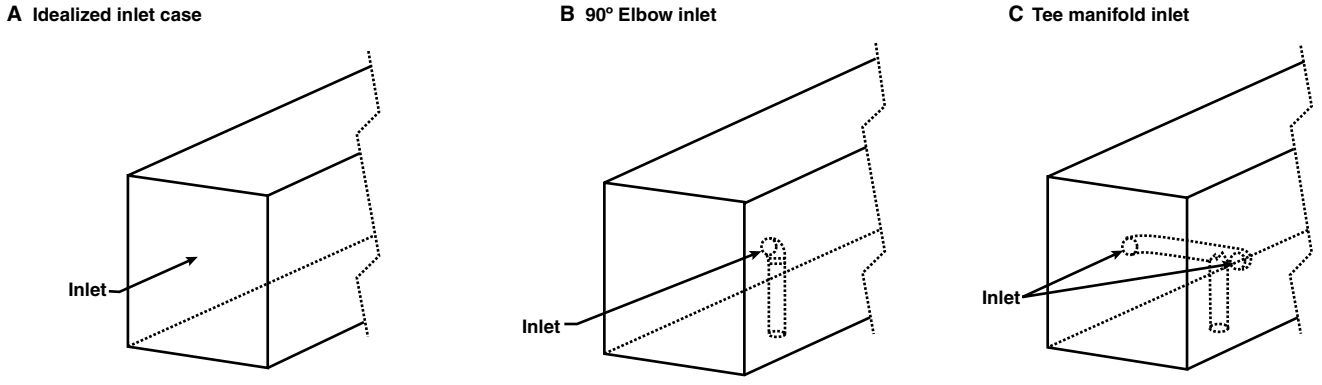

FIGURE 3 Baseline RTD curves for the Jamestown disinfection contact tank

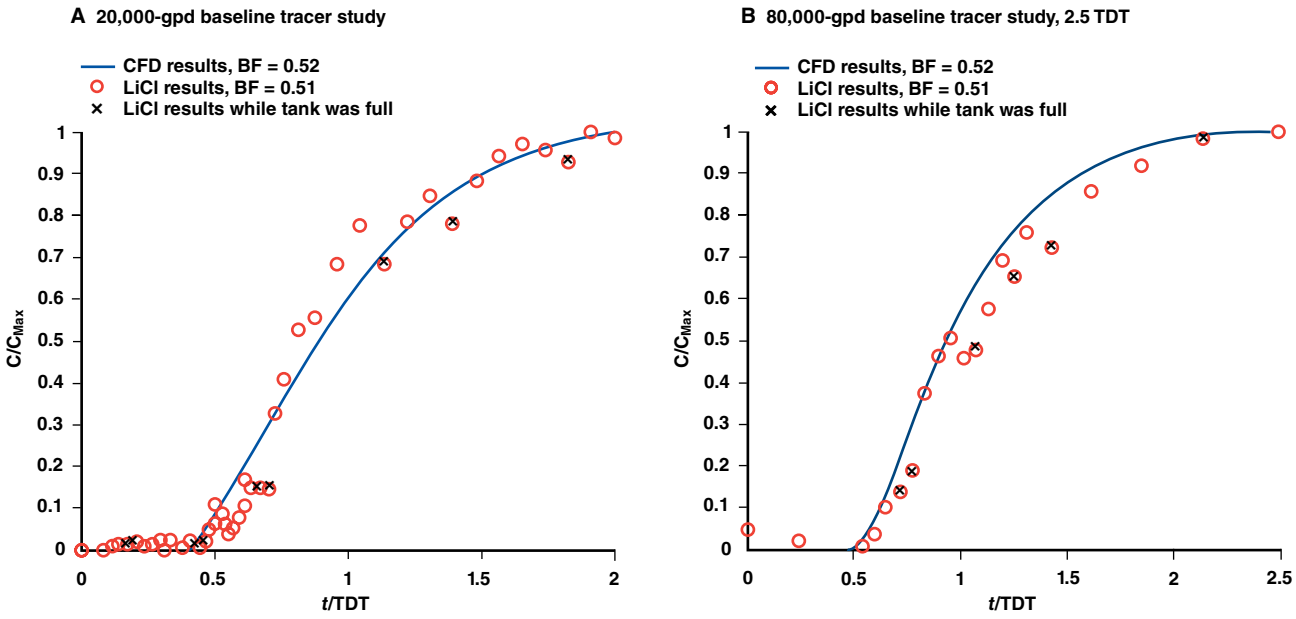

BF—baffling factor, CFD—computational fluid dynamics, LiCl—lithium chloride, RTD—residence time distribution, TDT—theoretical detention time

***C*/*C*$_{Max}$ is the measured concentration value of a tracer material at a given time, *t*, at the system outlet divided by the tracer's maximum concentration at the system outlet, and *t*/TDT is the contact time divided by the system's theoretical detention time.**

outlet weir into a collection tank before being pumped into the supply system. This collection tank had two service pumps that were activated by a float switch; however, this float switch would engage only when the weir became completely submerged.

When the weir was fully submerged, the water in the collection tank with a lower tracer concentration would mix with the water upstream of the weir with a higher concentration. This mixing diluted the upstream tracer concentration, a development that is evident in parts A and B of Figure 3. The points marked by a circled *x* were those taken when the weir was completely submerged. However, this anomaly did not significantly affect the results of the tracer studies. With the use of both the CFD and tracer results, it was determined that the BF of the system varied between 0.5 and 0.6. The high correlation and low root-mean-square errors (0.06 and 0.05 for parts A and B, respectively, of Figure 3) between the baseline RTD curves from the CFD model and tracer studies indicated good statistical fit and validated the CFD models used for this study. Given the good agreement between the physical tracer tests and CFD model results, the authors did not perform an in-depth CFD model sensitivity analysis (e.g., Peplinski & Ducoste, 2002). The CFD results plotted in Figure 3, part A, were generated with the laminar model because of the low Reynolds number of the flow and are discussed further in the next subsection.

TABLE 2 Reynolds numbers in the contact tank for the two operating flow rates

Flow Rate *gpd*	Average Tank Velocity *ft/min*	Reynolds Number
20,000	0.39	2,270
80,000	1.40	13,770

Laminar and turbulent flow models. The Reynolds numbers for the two flow rates were calculated using the results from the validated baseline CFD models and are shown in Table 2. It is clear that the flow within the contact tank was fully turbulent when the plant was operating at 80,000 gpd (3.5 L/s). However, when the flow rate dropped to 20,000 gpd (0.88 L/s) in the winter, the flow became primarily laminar even though the incoming jet might be considered turbulent. Essentially, the fluid surrounding the inflow jet can transition from turbulent to laminar conditions depending on the overall momentum of the incoming jet. A strong (highly turbulent) jet is able to mix and spread much more efficiently than a weaker jet at lower flow rates. This shift from a fully turbulent to a partially laminar flow regime significantly alters the internal velocity field in the contact tank, as is evident in parts A and B of Figures 4 and 5. Figure 4 depicts the flow velocities in the tank at 0.33 ft (10 cm) above the tank floor for flow rates of 20,000 gpd (0.88 L/s) and 80,000 gpd (3.5 L/s), parts A and B of the figure, respectively. Figure 5, parts A and B, shows the corresponding flow velocities in the tank at 1.6 ft (50 cm) above the tank floor. For purposes of comparison, the corresponding flow velocities for the idealized inlet case (Figure 2, part A) are shown in parts C and D of Figures 4 and 5. The velocity fields depicted in Figures 4 through 7 have been normalized by the average velocities for each scenario as shown in Table 3. Because of the geometry of the tank and the location of the inlet pipe, a jet appears to clearly form downstream of the inlet at both 20,000 gpd (0.88 L/s) and 80,000 gpd (3.5 L/s), as shown in Figure 4, parts A and B. However, the jet dissipates faster when the system is operating in the turbulent regime as shown in Figure 4, part B, and Figure 5, part B. At 20,000 gpd (0.88 L/s), the downstream jet did not contain enough turbulent energy to spread and mix effectively across the tank's cross section. Without the effects of turbulent mixing in the surrounding flow, the energy of this downstream jet was dissipated only when the flow contacted the back wall of the tank and turned around the baffle tip (as seen in Figure 4, part A).

Physical tank modifications. Table 4 shows the BFs from the CFD models of the baseline case, the 90-degree elbow inlet, the tee manifold inlet, and the idealized inlet for flow rates of 20,000 gpd (0.88 L/s) and 80,000 gpd (3.5 L/s). The results of the idealized case showed that the BF could theoretically be increased by 29% whereas the tee manifold shown in Figure 2, part C, helps to stabilize the BF at 0.62. The 19% increase in BF with the tee manifold from the baseline case for a flow rate of 20,000 gpd (0.88 L/s) was achieved because of the inlet's orientation, which helped to split the influent. Because the tee manifold had twice the inlet surface area of the baseline case, it was able to deliver the influent into the system with one quarter of the kinetic energy. This reduction of influent kinetic energy, coupled with the flow being dispersed via the front wall of the tank, created a velocity profile that was uniform, as shown in parts A and B of Figures 6 and 7. For

FIGURE 4 Planar view of flow velocity (0.33 ft above tank floor) for baseline case and idealized inlet

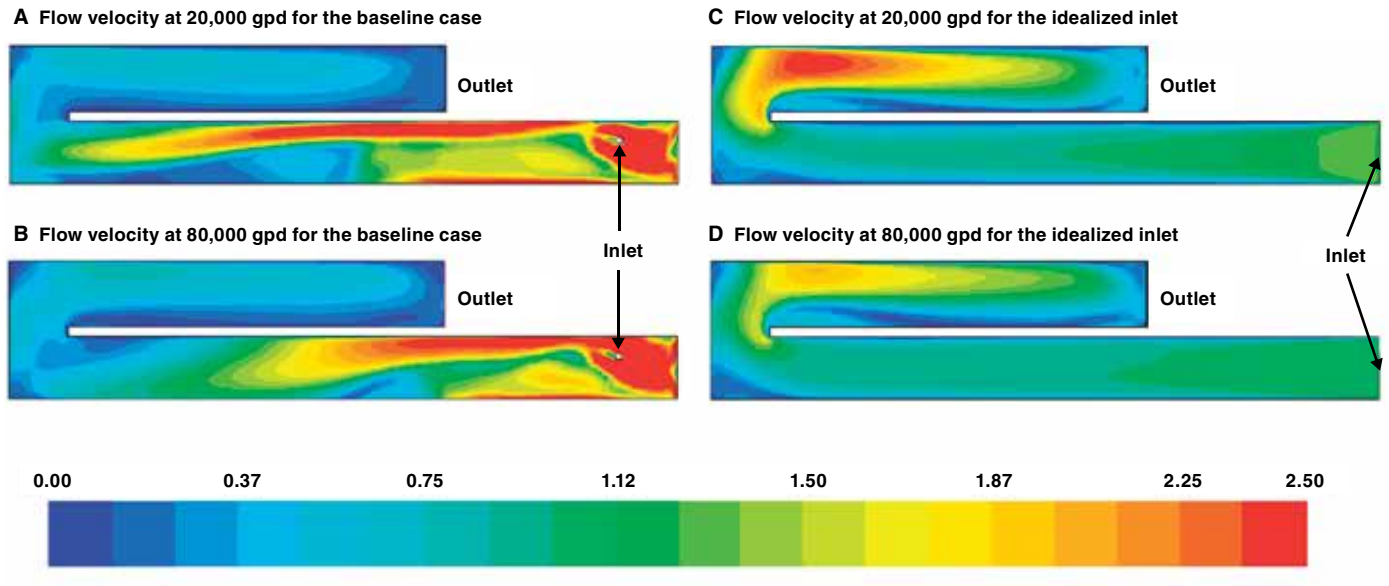

See Table 3 for the average velocities in ft/min that were used to normalize this figure.

FIGURE 5 Planar view of flow velocity (1.6 ft above tank floor) for baseline case and idealized inlet

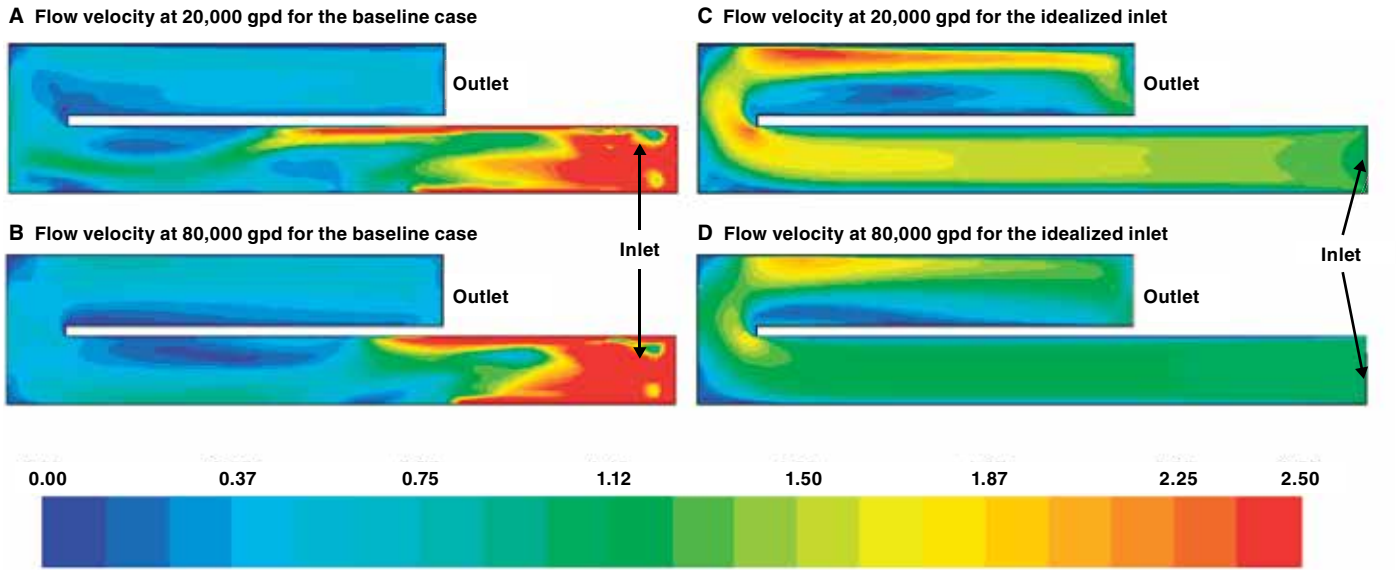

See Table 3 for the average velocities in ft/min that were used to normalize this figure.

comparison, the corresponding flow velocities for the idealized inlet case (Figure 2, part A) are shown in parts C and D of Figures 6 and 7. From the figures, it is evident that the downstream jet that plagued the baseline system (shown in parts A and B of Figures 4 and 5) has been completely mitigated.

CONCLUSION

Seasonal variations in the operations of water contact tanks can significantly affect the internal velocity fields and flow regime. As shown in this study, seasonal variations were capable of changing the Reynolds number of the flow by a factor of 6. It was found that such changes in the Reynolds numbers were great enough to shift the flow regime from turbulent to primarily laminar or vice versa. The effects of these seasonal variations could be compounded if the system were also thermally stratified, which can attenuate vertical mixing in the tank.

The study found that the BF of the baseline system decreased by 18% under partially laminar flow conditions. The system discussed in this research was designed so that it relied on turbulent diffusion to encourage pluglike flow by dissipating the influent energy from the incoming jet. The decrease in system performance was directly related to the inability of the incoming jet to spread and mix quickly across the tank's cross section. Installing a simple inlet manifold allowed the internal velocity fields and BF to stabilize during both high- and low-flow conditions. The proposed tee manifold inlet was able to create a uniform velocity field while reducing the volume lost to high-velocity zones for both flow rates. This was accomplished through the reduction and dissipation of the kinetic energy from the influent.

Although USEPA guidelines and design manuals are adequate for systems that operate only under turbulent flow conditions, care must be taken when designing a system that will encounter

TABLE 3 Average velocities used to normalize the velocity magnitude shown in Figures 4–7

System	Flow Rate *gpd*	Average Velocity *ft/min*
Baseline	20,000	0.39
	80,000	1.40
Tee manifold	20,000	0.24
	80,000	0.99
Idealized	20,000	0.17
	80,000	0.67

TABLE 4 BFs for the four inlet scenarios analyzed in this study

	20,000-gpd Flow Rate		80,000-gpd Flow Rate	
Inlet Condition	BF	% Increase	BF	% Increase
Baseline	0.52	0	0.63	0
90-degree elbow	0.56	7.7	0.65	3.2
Tee manifold	0.62	19.2	0.67	6.4
Idealized	0.67	28.9	0.75	19.1

BF—baffling factor

FIGURE 6 Planar view of flow velocity (0.33 ft above tank floor) for tee manifold and idealized inlets

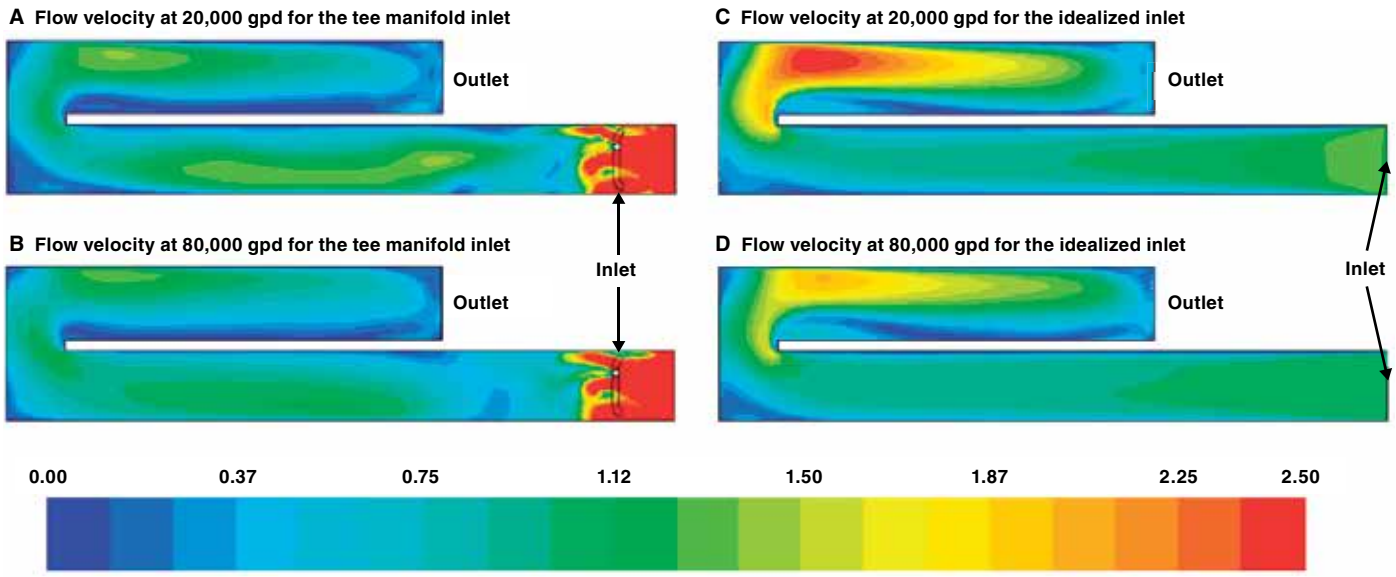

See Table 3 for the average velocities in ft/min that were used to normalize this figure.

FIGURE 7 Planar view of flow velocity (1.6 ft above tank floor) for tee manifold and idealized inlets

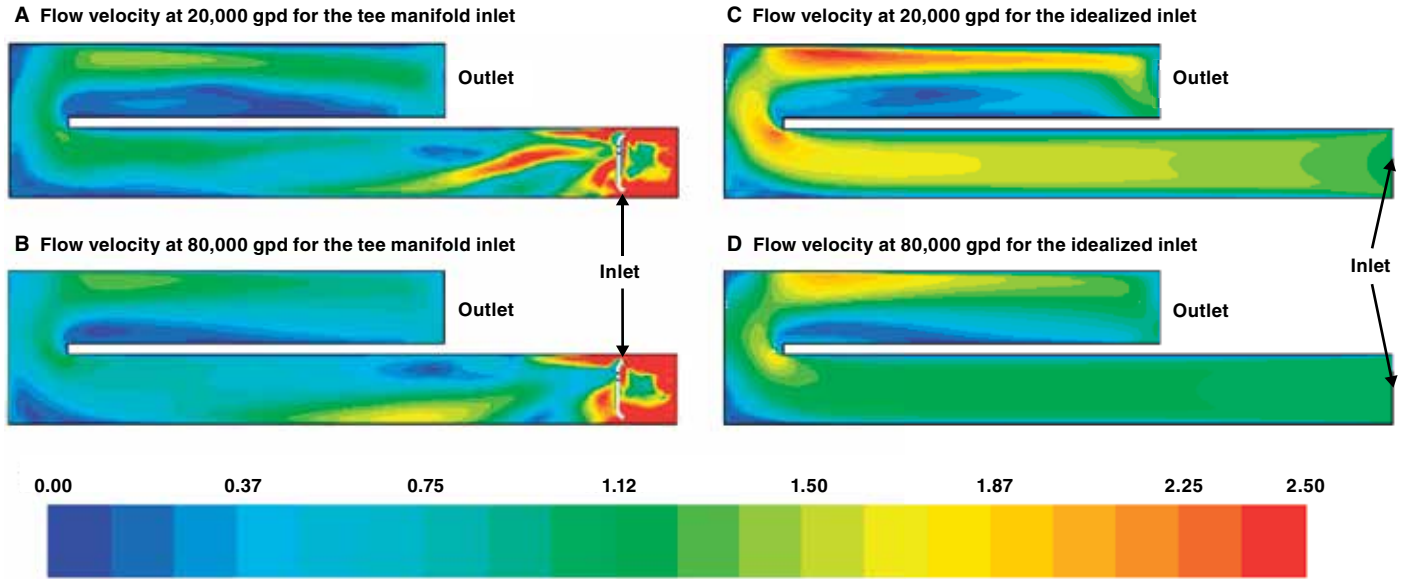

See Table 3 for the average velocities in ft/min that were used to normalize this figure.

laminar flow conditions. The current study showed that the mechanism by which influent energy is dissipated must be able to operate properly, regardless of flow regime. Systems that must operate under laminar flow conditions should be designed with larger inlets that are oriented in such a fashion that discourage the formation of any downstream jets. The findings of this study are directly relevant to small drinking water systems that are likely to operate under a range of flow conditions encompassing both turbulent and laminar flow regimes.

ACKNOWLEDGMENT

The authors would like to acknowledge the Colorado Department of Public Health and Environment Water Quality Division (Denver, Colo.) for funding of this project and Tyson Ingels,

Melanie Criswell, and Gordon Whittaker for their support. They also thank the city of Jamestown, Colo., for use of its water treatment facility and Jonathan Ashton and Emma Hardy of the water operations staff for their assistance. Finally, the authors thank Justin Kattnig for his help in conducting the tracer studies.

ABOUT THE AUTHORS

Taylor C. Barnett *is an engineering technical services consultant at Innovyze in Broomfield, Colo. At the time of the study described here, he was a graduate student in the Department of Civil and Environmental Engineering at Colorado State University, Fort Collins, Colo., from which he received bachelor and master of science degrees in civil engineering. As part of his thesis for his master's degree, Barnett conducted two years of research on the hydraulics of drinking water contact tanks.* ***Subhas K. Venayagamoorthy*** *(to whom correspondence should be addressed) is an associate professor in the Department of Civil and Environmental Engineering, Colorado State University, 1372 Campus Delivery, Fort Collins, CO 80523, vskaran@colostate.edu.*

PEER REVIEW

Date of submission: 12/28/2013
Date of acceptance: 08/11/2014

FOOTNOTE

[1]Fluent, version 13, ANSYS, Canonsburg, Pa.

REFERENCES

Amini, R.; Taghipour, R.; & Mirgolbabaei, H., 2011. Numerical Assessment of Hydrodynamic Characteristics in Chlorine Contact Tank. *International Journal for Numerical Methods in Fluids,* 67:7:885. http://dx.doi.org/10.1002/fld.2394.

ANSYS, 2011. *Fluent Theory Guide.* ANSYS, Canonsburg, Pa.

Baawain, M.S.; El-Din, M.G.; & Smith, D.W., 2006. Computational Fluid Dynamics Application in Modeling and Improving the Performance of a Storage Reservoir Used as a Contact Chamber for Microorganism Inactivation. *Journal of Environmental Engineering and Science,* 5:2:151. http://dx.doi.org/10.1139/s05-023.

Bradbrook, K.F.; Biron, P.M.; Lane, S.N.; Richards, K.S.; & Roy, A.G., 1998. Investigation of Controls on Secondary Circulation in a Simple Confluence Geometry Using a Three-Dimensional Numerical Model. *Hydrological Processes,* 12:1371. http://dx.doi.org/10.1002/(SICI)1099-1085(19980630)12:8<1371::AID-HYP620>3.0.CO;2-C.

Brouckaert, C.J. & Buckley, C.A., 1999. Use of Computational Fluid Dynamics for Improving the Design and Operation of Water and Wastewater Treatment Plants. *Water Science and Technology,* 40:4:81. http://dx.doi.org/10.1016/S0273-1223(99)00488-6.

Khan, L.A.; Wicklen, E.A.; & Teixeira, E.C., 2006. Validation of a Three-Dimensional Computational Fluid Dynamics Model of a Contact Tank. *Journal of Hydraulic Engineering,* 132:7:741. http://dx.doi.org/10.1061/(ASCE)0733-9429(2006)132:7(741).

Munson, B.R.; Okiishi, T.H.; Huebsch, W.W.; & Rothmayer, A.P., 2013. *Fundamentals of Fluid Mechanics.* Wiley, Hoboken, N.J.

Peplinski, D.K. & Ducoste, J.J., 2002. Modeling of Disinfection Contactor Hydraulics Under Uncertainty. *Journal of Environmental Engineering,* 128:11:1056. http://dx.doi.org/10.1061/(ASCE)0733-9372(2002)128:11(1056).

Pope, S.B., 2000. *Turbulent Flows.* Cambridge University Press, Cambridge, U.K. http://dx.doi.org/10.1017/CBO9780511840531.

Rauen, W.B.; Angeloudis, A.; & Falconer, R.A., 2012. Appraisal of Chlorine Contact Tank Modelling Practices. *Water Research,* 46:18:5834. http://dx.doi.org/10.1016/j.watres.2012.08.013.

Rouse, H., 1946. *Elementary Fluid Mechanics,* Wiley, New York, 1946.

Templeton, M.R.; Hofmann, R.; & Andrews, R.C., 2006. Case Study Comparisons of Computational Fluid Dynamics (CFD) Modeling Versus Tracer Testing for Determining Clearwell Residence Times in Drinking Water Treatment. *Journal of Environmental Engineering Science,* 5:6:529. http://dx.doi.org/10.1139/s06-007.

USEPA (US Environmental Protection Agency), 2011. National Characteristics of Drinking Water Systems Serving 10,000 or Fewer People. EPA 816-R-10-022, Office of Water, Washington.

USEPA, 2003. LT1ESWTR Disinfection Profiling and Benchmarking Guidance Manual. EPA 816-R-004, Office of Water, Washington.

USEPA, 1991. Guidance Manual for Compliance With the Filtration and Disinfection Requirements for Public Water Systems Using Surface Water Sources. EPA-68-01-6989, Office of Drinking Water, Washington.

Venayagamoorthy, S.K. & Stretch, D.D., 2010. On the Turbulent Prandtl Number in Homogeneous Stably Stratified Turbulence. *Journal of Fluid Mechanics,* 644:359.

Wang, H. & Falconer, R.A., 1998. Numerical Modeling of Flow in Chlorine Disinfection Tanks. *Journal of Hydraulic Engineering,* 124:9:918. http://dx.doi.org/10.1061/(ASCE)0733-9429(1998)124:9(918).

Wang, H.; Shoa, X.; & Falconer, R.A., 2003. Flow and Transport Simulation Models for Prediction of Chlorine Contact Tank Flow-Through Curves. *Water Environment Research,* 75:5:455. http://dx.doi.org/10.2175/106143003X141268.

Zhang, J.M.; Khoo, B.C.; Lee, H.P.; Teo, C.P.; Haja, N.; & Peng, K.Q., 2011a. Effects of Baffle Configurations on the Performance of a Potable Water Service Reservoir. *Journal of Environmental Engineering,* 138:5:578. http://dx.doi.org/10.1061/(ASCE)EE.1943-7870.0000502.

Zhang, J.M.; Lee, H.P.; Khoo, B.C.; Teo, C.P.; Haja, N.; & Peng, K.Q., 2011b. Modeling and Simulations of Flow Pattern, Chlorine Concentration, and Mean Age Distributions in Potable Water Service Reservoir of Singapore. *Journal of Environmental Engineering,* 137:7:575. http://dx.doi.org/10.1061/(ASCE)EE.1943-7870.0000359.